AIAA JOURNAL
Vol. 36, No. 10, October 1998

Characterization of the Pressure Fluctuations Under a Fully Developed Turbulent Boundary Layer

S. P. Gravante,* A. M. Naguib,† C. E. Wark,‡ and H. M. Nagib‡
Illinois Institute of Technology, Chicago, Illinois 60616

Accurate measurements of the turbulent wall pressure have been difficult to achieve due to signal contamination at low frequencies by background facility noise and/or attenuation at high frequencies due to sensor averaging effects. The current study utilizes a new noise cancellation scheme based on an optimal filtering technique to capture the noise-canceled time series. Furthermore, to address the high-frequency attenuation problem, a number of pinholes are utilized along with high-sensitivity microphones to obtain measurements of the wall pressure at a resolution down to $d^+ = du_\tau/\nu \cong 2$. The results show that the maximum allowable nondimensional sensing diameter to avoid spectral attenuation for frequencies up to $f^+ = f\nu/u_\tau^2 = 1$ is in the range of $12.0 \le d^+ < 18.0$. Additionally, it is shown that the wall-pressure rms level when scaled on the wall-shear stress seems to increase slowly with increasing Reynolds number, apparently due to the influence of large-scale structures in the outer part of the boundary layer. On the other hand, it is demonstrated that, even though $\sqrt{p'^2}/q_0$ appears to become invariant with increasing Reynolds number, p' is not generated by structures whose velocity scale is U_0.

Nomenclature

d^+	= nondimensional microphone sensing diameter, du_τ/ν
f	= frequency
K	= kurtosis
$\sqrt{p'^2}$	= rms of the pressure fluctuations
q_0	= dynamic pressure, $\frac{1}{2}\rho U_0^2$
Re_θ	= Reynolds number based on momentum thickness, $U_0\theta/\nu$
Re_τ	= Reynolds number based on friction velocity and boundary-layer thickness, $u_\tau\delta/\nu$
S	= skewness
U_0	= free stream velocity
u_τ	= wall-friction velocity $(\tau_w/\rho)^{1/2}$
x	= streamwise coordinate
y	= wall-normal coordinate
$\Delta\omega^+$	= angular frequency resolution normalized with the inner timescale
δ	= boundary-layer thickness
θ	= momentum thickness
ρ	= density
τ_w	= average (mean) wall-shear stress
$\phi_{p'p'}$	= power-spectral density of wall-pressure fluctuations
$\phi^o_{p'p'}$	= power-spectral density scaled on outer variables, $\phi_{p'p'}u_\tau/\tau_w^2\delta$
$\phi^+_{p'p'}$	= power-spectral density scaled on inner variables, $\phi_{p'p'}u_\tau^2/\tau_w^2\nu$
ϕ_{vv}	= power-spectral density of uncalibrated voltage time series
ω	= angular frequency, $2\pi f$
ω^o	= angular frequency normalized with the outer timescale, $\omega\delta/u_\tau$
ω^+	= angular frequency normalized with the inner timescale, $\omega\nu/u_\tau^2$

I. Introduction

TURBULENT pressure fluctuations play a significant role in many engineering applications. For example, pressure fluctuations in a turbulent boundary layer over an airplane wing or cabin can produce unwanted structural vibrations, and/or they can be a source of undesired acoustic noise. These problems serve as the motivating factor in studying turbulent wall-pressure fluctuations and their relationship to the turbulent flowfield.

A. Measuring Turbulent Wall-Pressure Fluctuations

One difficulty in accurately measuring turbulent wall-pressure fluctuations is the effect of freestream disturbances. Even for acoustically quiet tunnels, measurements of wall-pressure fluctuations are susceptible to contamination by long-wavelength acoustic noise generated by the wind-tunnel fan or blower and flow unsteadiness, e.g., see Ref. 1. These acoustic disturbances typically appear as peaks in the wall-pressure spectrum at frequencies corresponding to the blade passing frequency of the tunnel fan and/or as standing waves in the test section of the wind tunnel. The acoustic noise, regardless of its source, is superimposed onto the wall-pressure fluctuations masking the turbulent signal. This problem is typically overcome by high-pass filtering the signal to remove the frequency region contaminated by acoustic noise. However, this method removes information regarding the large-scale turbulent structures and should not be used when this information is desired.

A second method to deal with the unwanted noise has been a two-transducer subtraction technique. This method has been used for several decades and was first introduced by Wambsganss and Zaleski.[2] The scheme is based on subtracting two wall-pressure time series and requires that only the acoustic noise is correlated between the two transducers. This technique, however, provides information regarding only the second-order statistics and does not provide the turbulent wall-pressure time series.

Alternatively, many investigations have made measurements at Reynolds numbers high enough such that the turbulent energy content is large with respect to the energy of the acoustic noise. As a result, there is an insufficient number of low-Reynolds-number measurements to which direct numerical simulation (DNS) results can be compared. Such a comparison would be invaluable for the development of turbulence models. Specifically, DNS studies provide information for validating models of quantities that are not easily measured experimentally, such as the pressure–strain correlation. Once validated, these models could be adapted to practical applications using experiments ranging from the low Reynolds numbers achievable in DNS studies to the high Reynolds numbers encountered in practical applications.

In addition, because the range of the scales of motion increases with increasing Reynolds number and, in most instances, the size of the small-scale structures decreases, many high-Reynolds-number

Received July 30, 1997; revision received April 1, 1998; accepted for publication July 2, 1998.

*Research Assistant, Department of Mechanical, Material, and Aerospace Engineering, Fluid Dynamics Research Center. Student Member AIAA.

†Research Assistant Professor, Department of Mechanical, Material, and Aerospace Engineering, Fluid Dynamics Research Center. Member AIAA.

‡Professor, Department of Mechanical, Material, and Aerospace Engineering, Fluid Dynamics Research Center. Member AIAA.

measurements of turbulent wall-pressure fluctuations suffer from poor spatial resolution. It is known that, to accurately resolve the small-scale structures of a turbulent boundary layer, the size of the transducer must be as small as the smallest turbulent structures. For transducers whose size is large with respect to the smallest scales of motion, the turbulent signal is attenuated because the transducer effectively low-pass filters the high-frequency component of the signal corresponding to the smallest turbulent structures.

B. Review of Pertinent Literature

Three good reviews on the experimental investigations of turbulent wall-pressure fluctuations are provided by Willmarth,[3] by Eckelmann,[4] and most recently by Bull.[5] However, it is still important to highlight some of the more significant work to which the current study will make comparisons, especially in the areas of sensor size effects and the characteristics of turbulent wall-pressure spectra.

Several studies have examined the effect of spatial averaging on wall-pressure measurements, but the most notable experimental work has been by Schewe.[6] In Ref. 6, Schewe studied the effect of spatial averaging on the wall-pressure statistics such as spectra, rms level, and the probability density function. Schewe suggested that the largest allowable value of the nondimensional sensing diameter of a transducer that can resolve the significant turbulent scales of motion was $d^+ = du_\tau/\nu = 19$. However, Schewe made this determination not by direct measurement but by extrapolating from data obtained at $d^+ = 19$ (which was the smallest sensor used in Schewe's investigation) to an infinitesimally small transducer, i.e., $d^+ = 0$.

Lueptow[7] numerically applied a wave number filter corresponding to the spatial response function of finite-size circular and square transducers to the DNS channel flow results of Kim et al.[8] Using the available time steps of the DNS database, Lueptow[7] was able to estimate the wall-pressure spectrum for various transducer sizes. These spectra showed insignificant wall-pressure energy attenuation for transducer sizes less than 20 viscous units.

Recently, Löfdahl et al.[9] used a new type of wall-pressure sensor based on microelectromechanical systems (MEMS) technology to conduct measurements of the wall pressure. With the MEMS technology they were able to construct two miniature piezoresistive sensors with a square diaphragm measuring 100 and 300 μm on the side.[9] The corresponding nondimensional diaphragm size was 7.2 and 21.6 in wall units at a boundary-layer Reynolds number Re_θ of 5072. Löfdahl et al.[9] showed that the wall-pressure spectrum measured with the larger sensor was attenuated for frequencies higher than approximately 1000 Hz. The resulting attenuation in the total wall-pressure rms value was about 8%.

Investigation of the scaling of the turbulent wall-pressure spectra is a widely used method for determining locations of sources within the boundary layer that are responsible for the generation of the wall-pressure fluctuations. The most recent study implementing this technique is by Farabee and Casarella,[1] where the spectra are shown to collapse to a single curve on both inner and outer variables over the middle range of frequencies. They attribute this region of overlap to turbulence activity in the log layer of the boundary layer. Also, Farabee and Casarella show that the spectra collapse when scaled on outer variables for the low-frequency range and on inner variables for the high-frequency range. Note, however, that the measurements of Farabee and Casarella were made with sensors whose size is larger than $d^+ = 26$.

The behavior of the wall-pressure spectrum has been predicted using scaling arguments by various researchers. Some of the more significant contributions to this area have been by Bradshaw[10] and Panton and Linebarger,[11] where it was predicted that the spectrum should obey a power law behavior of ω^{-1} over the frequency range where the spectra collapse on both inner and outer variables. Panton[12] discusses the Reynolds number dependence of the overlap region and identifies the locations of turbulent sources contributing to the overlap region. Other predicted power law features of the turbulent spectra include an $\omega^{-7/3}$ behavior for the range $0.4 \leq \omega^+ \leq 0.8$ by Monin and Yaglom[13] and ω^{-5} behavior by Blake[14] for the highest frequencies in the spectrum.

C. Objectives

The current study employs a new methodology to remedy the classical problems that occur when measuring the turbulent wall-pressure fluctuations (as discussed in Sec. I.B). 1) Specifically, to avoid low-frequency acoustic noise contamination of the transducer signal, a new noise cancellation scheme is utilized to remove the background tunnel noise at low frequencies while providing the noise-canceled time series. For the details of the noise cancellation technique, see Ref. 15. 2) To avoid spatial averaging effects at the higher Reynolds numbers, a combination of highly sensitive microphones and pinholes is used to obtain measurements of the turbulent wall-pressure fluctuations with a resolution of $d^+ \approx 2$. Note that pinholes have been used by other researchers, e.g., Bull and Thomas[16] and Farabee and Casarella,[1] as a means for decreasing the sensing area of the microphone and thereby increasing its spatial resolution. Our main objective is to use this new methodology to obtain accurate measurements of the turbulent wall pressure. It will then be possible to verify the results of earlier studies, which may suffer from one or more of the problems mentioned.

Specifically, the Reynolds number effect on the rms level, skewness, and kurtosis will be examined and compared with previously published results. Also, the characteristics of the turbulent wall-pressure spectra will be examined, including scaling and power law behavior.

II. Experimental Facility

The experiments were conducted in the Mark V. Morkovin Wind Tunnel at the Illinois Institute of Technology. The reader is referred to Ref. 17 for a description of the wind tunnel and the boundary-layer test plate.

A. Instrumentation

Measurements of the wall pressure are made under a zero pressure gradient, flat plate, fully turbulent boundary layer with a low freestream turbulence of less than 0.3%. This value includes both acoustic and turbulence effects. Farabee and Casarella[1] have shown that, even in their low-noise facility, the major source contaminating measurements of the wall pressure is the acoustic, rather than the turbulence, freestream fluctuations. Also note that freestream turbulence influences on the wall-pressure spectrum are anticipated to scale with U_0. As will be seen later, at no frequency in the measured wall-pressure spectra does U_0 represent the appropriate velocity scale. Again, this suggests that freestream turbulence has negligible, if any, effects on the current results.

The pressure measurements are done using a Knowles EM-3068 Electret microphone. The microphone has a 0.7-mm sensing diameter, which minimizes signal attenuation due to spatial averaging effects. The microphone also has a high acoustic sensitivity that typically measures about 15 mV/Pa at 1000 Hz. (Note that this is approximately 10 times more sensitive than a typical Brüel and Kjaer $\frac{1}{4}$-in. microphone.) This high sensitivity allows the microphone to detect the extremely small turbulent pressure fluctuations, whose rms level is on the order of 100 mPa at low Reynolds numbers.

The main disadvantage of the EM-3068 microphone is that it has a nonuniform frequency response. The microphone's response is flat (within 5 dB) from 1000 to 5000 Hz but is attenuated outside this region. In addition, no phase response for the Knowles EM-3068 microphone is available. This requires that the EM-3068 microphone be dynamically calibrated to account for variations in its sensitivity and phase with frequency. The calibration procedure follows the one used by Snarski[18] with modifications to enhance its accuracy and range, as described by Gravante.[19] The method simply uses a microphone of known amplitude and phase response to calibrate a microphone of unknown amplitude and phase response by exposing both microphones simultaneously to the same sound field. Provided that the amplitude of the incoming sound wave is the same at both microphones and relative phase difference between them is zero, the method is capable of dynamically calibrating the unknown microphone. Because of limitations in the signal-to-noise ratio, the calibration procedure is valid only in a frequency range from 35 to about 12,000 Hz.

Figure 1a is the amplitude response of a Brüel and Kjaer (B&K) 4193 $\frac{1}{2}$-in. microphone obtained using the calibration procedure

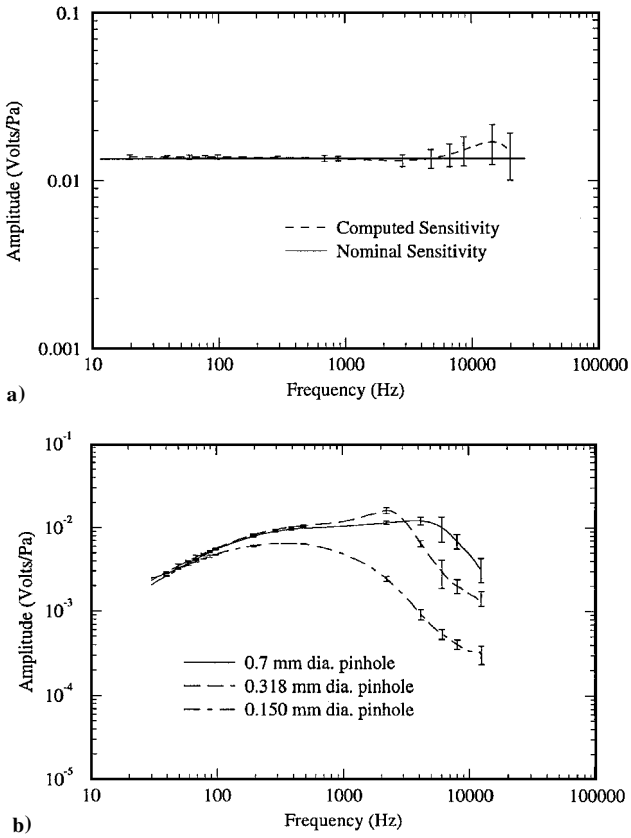

Fig. 1 Comparison of the a) calibrated amplitude response of the B&K 4193 microphone with factory-specified calibration curve and b) calibrated amplitude response of the Knowles EM-3068 microphone for various pinhole sizes.

already briefly described. Also plotted is the factory-measured response of that same microphone. The close agreement between the two curves indicates the capability of the calibration procedure to measure the amplitude response of the microphone accurately. Figure 1b gives the amplitude response of the Knowles EM-3068 microphone with a 0.7-, 0.318-, and 0.150-mm sensing diameter. The error bars represent the uncertainty in the amplitude response with a 90% confidence level using a Gaussian distribution, where the standard deviation is computed from 10 independent measurements.

B. Experimental Setup and Procedure

The experimental setup consists of two Knowles EM-3068 microphones mounted flush with a flat plate in one of three removable wall plugs. The microphones are placed at the same streamwise location but separated in the spanwise direction by 63.5 mm for all measurements made during this investigation. The number of microphones and the spanwise separation distance are chosen to meet the requirements of the noise cancellation procedure described in Naguib et al.[15]

Measurements of the wall-pressure fluctuations under a turbulent boundary layer are obtained for the range of Reynolds numbers $1577 \leq Re_\theta \leq 7076$, which are shown in Table 1 along with the corresponding boundary-layer parameters and data acquisition frequencies. Note that the boundary-layer parameters are based on measurements by Naguib.[20]

To ensure that the Reynolds number effect observed in the current results is free from sensor averaging effects, the measurements are repeated for different microphone sensing diameters. This is accomplished by placing the Knowles EM-3068 microphone under pinholes of varying size. The pinholes are carefully designed such that the Helmholtz resonance frequency is not located in the frequency range of interest and the pinhole itself does not introduce significant disturbances into the flow. In addition, any effect the pinhole may have on the frequency response of the microphone in both amplitude and phase is accounted for in a dynamic calibration procedure described by Gravante.[19] The following cases are studied

Table 1 Boundary-layer parameters for Reynolds numbers covered in this experiment[a]

Re_θ	x, m	U_0, m/s	u_τ, m/s	θ, mm	δ, mm	f_{acq}, Hz
1,577	3.25	4.8	0.22	5.0	49.4	3,200
1,805	2.49	6.6	0.28	4.3	41.3	6,300
1,955	3.86	4.7	0.21	6.2	57.5	3,200
2,953	3.25	7.2	0.29	6.3	54.8	6,300
2,972	3.86	6.5	0.27	6.9	61.1	6,300
3,509	2.49	10.6	0.41	5.2	45.8	10,000
4,548	3.25	10.7	0.40	6.6	58.4	10,000
4,972	2.49	15.7	0.58	5.0	44.9	25,000
4,986	3.86	10.4	0.40	7.3	63.8	10,000
6,241	3.25	15.7	0.57	6.2	53.9	25,000
7,076	3.86	15.3	0.57	7.0	62.9	25,000

[a]Parameters based on measurements by Naguib.[20]

Table 2 Nondimensional microphone sensing diameters (d^+) covered in this investigation

Re_θ	0.7 mm	0.318 mm	0.150 mm
1577	10.1	4.6	2.2
1805	12.9	5.8	2.8
1955	9.6	4.4	2.1
2953	13.3	6.0	2.9
2972	12.4	5.6	2.7
3509	18.8	8.5	4.0
4548	18.3	8.3	3.9
4972	26.6	12.1	5.7
4986	18.3	8.3	3.9
6241	26.2	11.9	5.6
7076	26.2	11.9	5.6

for the Reynolds number range given in Table 1: 0.7-, 0.318-, and 0.150-mm-diam pinhole. The corresponding range of nondimensional sensing diameter is $2 < d^+ < 27$ and is given in Table 2 as a function of Reynolds number.

C. Data Processing and Experimental Uncertainty

All time series used in computing the turbulent statistics were 409,600 points in length and were antialiased filtered at the Nyquist frequency. The power spectrum was computed using 200 ensembles, each 2048 points long, which provides a spectrum frequency resolution $\Delta\omega^+$ of about 0.005. The probability density function (PDF) was computed using 100 bins, with width of $4\sqrt{p'^2}/100$. The selection of the number of records for spectrum averaging and the number of bins for PDF estimation were such that the scatter in the results was comparable with other published data, e.g., see Fig. 2.

The momentum thickness is an integral quantity whose uncertainty is less than 1%. The friction velocity was obtained using a Clauser fit, the uncertainty of which is approximately ±3%. This uncertainty is based on a parametric study by Hites[21] of the random uncertainty in u_τ obtained using the Clauser fit procedure. The boundary-layer thickness was obtained by using a spline fit to the mean velocity profile and determining the location where the velocity was $0.995U_0$. Uncertainty in the turbulent wall-pressure spectrum is primarily due to the statistical convergence error, which is inversely proportional to the number of ensembles used in spectral averaging and the error in determining the transfer function of the Knowles microphone. This uncertainty is largest at frequencies greater than 10,000 Hz, where it is approximately ±7% (see Fig. 1).

Finally, two types of error bars appear in the figures containing the rms, skewness, and kurtosis: 1) error bars showing the minimum and maximum values of the plotted quantity obtained from three independent measurements and 2) error bars representing the uncertainty for 90% confidence level using a Student-t distribution along with the standard deviation in the measured quantity (based on three independent measurements). As will be seen, the latter type of error estimate tends to be more conservative to account for using only three independent observations in estimating the standard deviation of repeated trials of the same measurement. Also, both error bars could be viewed as providing the bounds on the actual

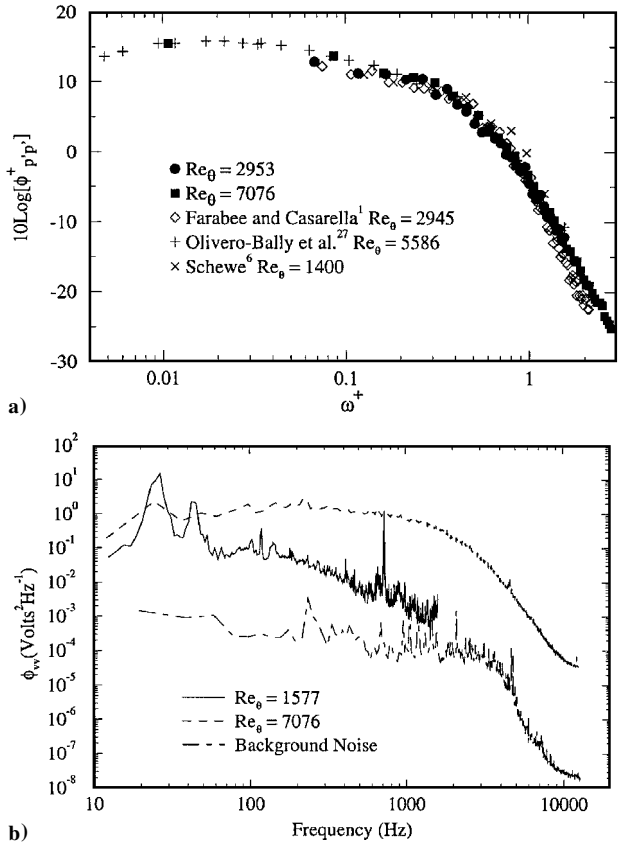

Fig. 2 Comparison of a) the spectra obtained in the current investigation to that of previous researchers at comparable Reynolds numbers and b) the signal and noise spectra for the smallest and largest Reynolds numbers in this study.

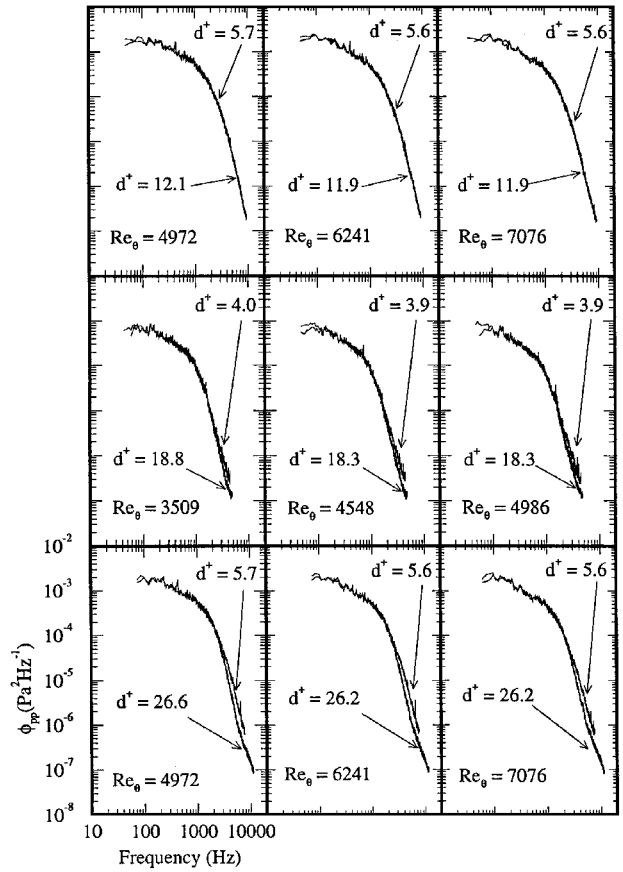

Fig. 3 Comparison of the PSD measured with $d^+ = 12.0$ (top row), $d^+ = 18.0$ (middle row), and $d^+ = 26.0$ (bottom row) to that obtained with $d^+ < 6.0$ under the same flow conditions.

uncertainty in the repeatability of the measurements under the same flow conditions.

III. Results and Discussion

A. Spatial Averaging Effects on Turbulent Wall-Pressure Statistics

It has been known for some time that the ratio of the sensing diameter of a pressure transducer to the smallest length scale in the flow should be as small as possible to minimize the effects of signal attenuation due to spatial averaging. Signal attenuation occurs when the size of the pressure transducer is large with respect to the length scale of the dynamically important turbulent structures. Specifically, the transducer acts as a low-pass filter where the high-frequency region of the spectrum corresponding to the smallest turbulent structures is attenuated because the energy contribution of the small scales is averaged over the surface of the transducer.

The current investigation complements the work of Schewe[6] by extending the range of sensing diameters over which the turbulent wall-pressure fluctuations are measured. The range of nondimensional sensing diameters covered in this investigation is $2 < d^+ < 27$, which overlaps the range covered by Schewe, $19 \leq d^+ \leq 333$.

To understand the effects of signal attenuation due to spatial averaging on the shape of the spectrum, it is useful to compare the power spectral density (PSD) obtained at the same flow conditions but with variously sized transducers. Figure 3 shows the PSD of the turbulent wall-pressure fluctuations measured with three sensing diameters: $d^+ \approx 26.0$ (bottom row), $d^+ \approx 18.0$ (middle row), and $d^+ \approx 12.0$ (top row). Also plotted is the spectrum obtained at the same flow conditions but with the smallest pinhole used in this investigation. The sensing diameter of these spectra is less than 6.0 for all cases. From Fig. 3, it can be seen that the spectra obtained at $d^+ \approx 26.0$ are attenuated for frequencies $f > 2000$ Hz relative to the spectra obtained at $d^+ \approx 5.6$. The same trend is evident in the spectra obtained at $d^+ \approx 18.0$, but it is not nearly as significant. Finally, there is no visible difference in the spectra obtained at $d^+ \approx 12.0$ relative to the spectra obtained at $d^+ \approx 5.6$. Therefore, it can be concluded that the smallest transducer required to measure the spectrum with no signs of spatial averaging effects is in the range $12.0 \leq d^+ < 18.0$. However, because the spectral attenuation at $d^+ = 18$ is barely detectable, to observe the proper scaling of the turbulent wall-pressure spectra, e.g., the spectra collapse to a single curve when scaled on inner variables, it is sufficient to measure the spectra with $d^+ \leq 18.0$. This conclusion is in agreement with the results of Lueptow[7] and Schewe.[6]

Figure 4a shows the wall-pressure spectrum for $Re_\theta = 7076$ plotted in a semilog format: $f\phi_{p'p'}(f)$ vs $\log_{10}(f)$. By plotting the spectrum in this way, it can be shown that the area under the curve is p'^2. This plotting format allows one to visually determine the fraction contribution to p'^2 from different frequency ranges. From Fig. 4a, it can be seen that, for frequencies larger than 2000 Hz, the spectral attenuation due to spatial averaging effects results in a reduction in area under the spectrum measured with $d^+ = 26.0$, when compared to the area under the spectrum corresponding to $d^+ = 11.9$ and 5.6. However, this area reduction is barely observable, and therefore, it may be concluded that, though spatial averaging has an effect on the shape of the spectrum at high frequencies, as seen in Fig. 3, its effect on the total energy content of the turbulent wall-pressure signal is negligible for $d^+ < 27.0$.

To understand the effects of spatial averaging on higher-order statistics of the wall pressure, it is useful to examine the effect spatial averaging has on the PDF. It is known that the higher-order statistics (skewness and kurtosis) are strongly influenced by the tails (large deviations from the mean value) of the PDF; therefore, by observing changes in the tails of the PDF for different nondimensional sensing diameters, the effect on the skewness and kurtosis may be inferred. Figure 4b shows the PDF at $Re_\theta = 7076$ corresponding to the 0.7-, 0.318-, and 0.150-mm pinhole cases, whose respective nondimensional sensing diameters are 26.2, 11.9, and 5.6. A Gaussian PDF is included in Fig. 4 for comparison purposes. From Fig. 4, it can be seen that there is close agreement among the PDFs for all nondimensional sensing diameters considered in this investigation. Therefore, it appears that spatial averaging has a minimal effect on the PDF and the associated higher-order statistics for $d^+ < 27.0$.

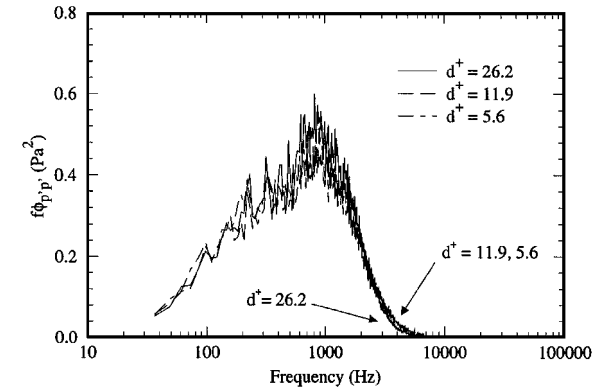

a) PSD in semilog format

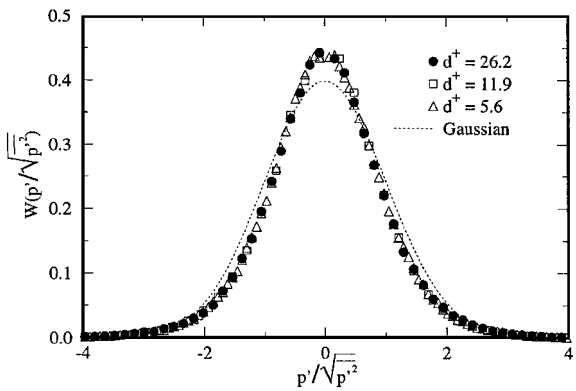

b) PDF

Fig. 4 $Re_\theta = 7076$ **with** $d^+ = 5.6$, **11.9, and 26.2.**

Comparing the negative tail of the PDF of the wall-pressure fluctuations to the positive one, there is no significant difference in the probability levels. This implies that the skewness of the wall-pressure signal is close, if not equal, to zero. Finally, comparing the tails of the PDF of the turbulent wall-pressure fluctuations to the PDF of a Gaussian-distributed random variable, it can be seen that large amplitude as well as very small amplitude fluctuations of the wall-pressure signal occur more frequently than in the case of a Gaussian-distributed random variable. Hence, the kurtosis of the wall-pressure fluctuations is expected to be larger than that of a Gaussian random variable ($K = 3.0$). The skewness and kurtosis will be discussed in more detail in the next section.

B. Reynolds Number Effect on Turbulent Wall-Pressure Statistics

Having demonstrated that spatial averaging does not significantly affect the wall-pressure statistics for the range of d^+ values covered here, it is now possible to interpret any observed changes in the statistics with Reynolds number based on momentum thickness Re_θ as being only due to changes in Reynolds number. This is unlike the work by Karangelen et al.,[22] Farabee and Casarella,[1] and Bull and Thomas,[16] where the effects of spatial averaging and Reynolds number were coupled, making it unclear whether changes in the statistical quantities with Reynolds number based on momentum thickness Re_θ were solely a Reynolds number effect or due, in part, to a spatial averaging effect.

The Reynolds number variation of $\sqrt{p'^2}$ has been discussed in detail by Farabee and Casarella[1] and more recently by Bull.[5] Figure 5a shows $\sqrt{p'^2}$ normalized by the dynamic pressure $q_0 = \rho U_0^2/2$ and plotted as a function of Reynolds number based on momentum thickness Re_θ. Note that the dashed lines in Fig. 5 (and in Figs. 6 and 7) represent the minimum and maximum values obtained from three independent measurements, whereas the error bars represent the uncertainty for a 90% confidence level (see Sec. II.C for more details). Figure 5 also contains data from Schewe,[6] Karangelen,[23] Farabee and Casarella,[1] and Bull and Thomas[16] for comparison. Schewe's results were obtained from measurements at a single Reynolds number for variously sized transducers, but only the result obtained with a sensor size of $d^+ = 19$ is shown. The data of Karangelen,[23]

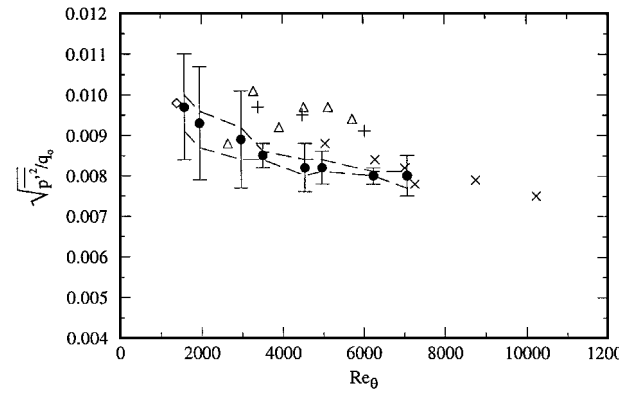

Fig. 5a RMS values of the wall-pressure fluctuations scaled on the dynamic pressure.

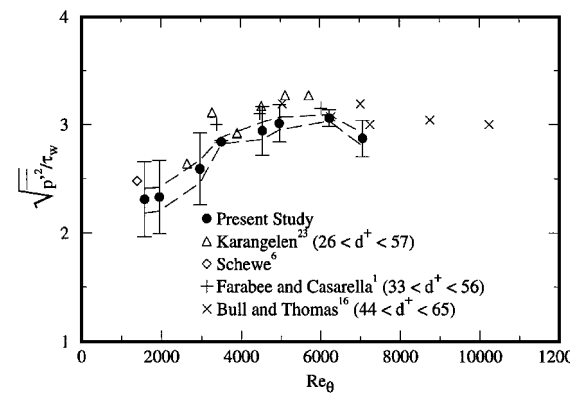

Fig. 5b Wall-shear stress as a function of Reynolds number based on momentum thickness Re_θ.

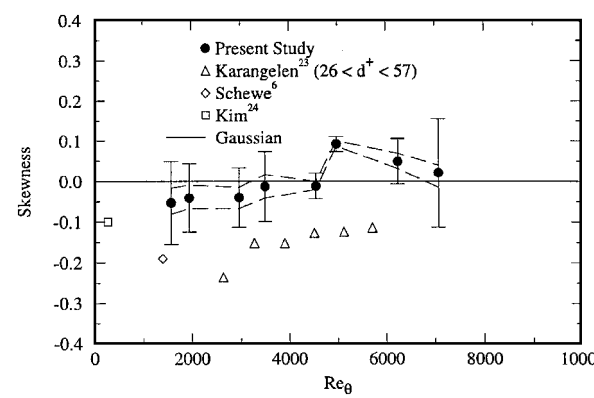

Fig. 6a Skewness of the turbulent wall-pressure fluctuations as a function of Reynolds number based on momentum thickness Re_θ.

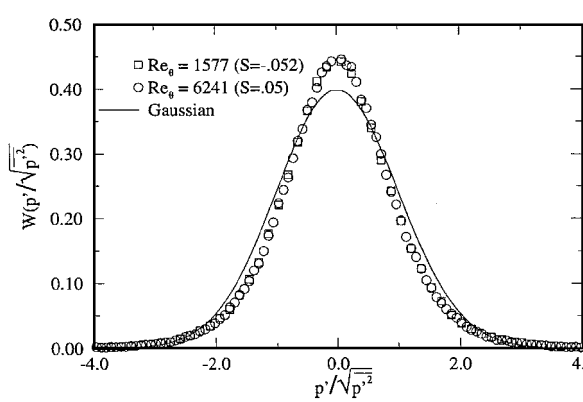

Fig. 6b PDF with small positive and negative skewness.

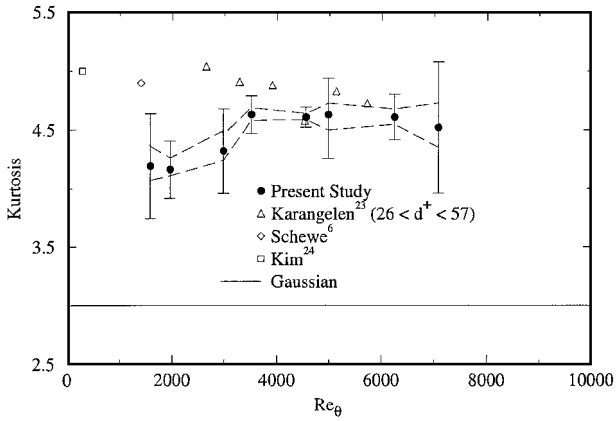

Fig. 7 Kurtosis of the turbulent wall-pressure fluctuations as a function of Reynolds number based on momentum thickness Re_θ.

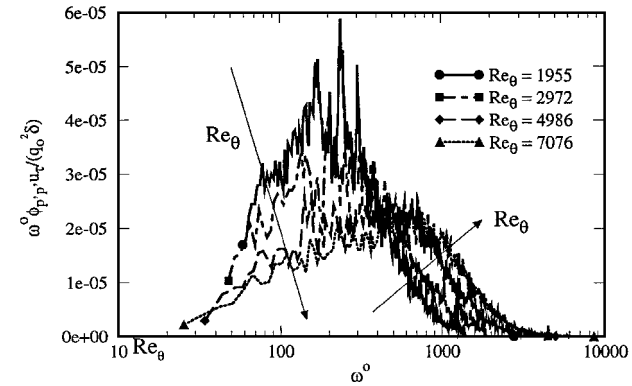

Fig. 8a Wall-pressure spectra plotted in semilog format to examine the scaling of $\sqrt{p'^2}$ on the dynamic pressure.

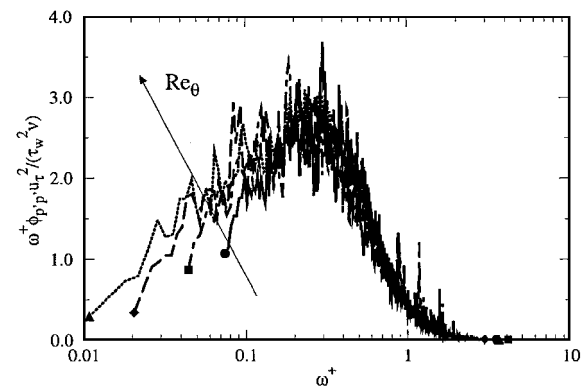

Fig. 8b Wall-shear stress.

Farabee and Casarella,[1] and Bull and Thomas[16] were obtained at various Reynolds numbers while the size of the transducer was kept constant. Hence, for those studies the nondimensional size of the transducer increases with increasing Reynolds number.

Upon comparison of the different data sets shown in Fig. 5a, it can be seen that the results from the current study are generally in agreement with those of previously published results. In addition, because the data set of the present study does not suffer from significant spatial averaging effects, as demonstrated in Figs. 3 and 4, a Reynolds number trend can be inferred, and it is shown that the quantity $\sqrt{p'^2}/q_0$ appears to become invariant with increasing Reynolds number. Figure 5b shows the same data as in Fig. 5a but with the rms of the turbulent wall-pressure fluctuations normalized by the wall-shear stress τ_w. As observed in Fig. 5b, the data of the present investigation are in good agreement with those of previously published results and show a slow variation with increasing Reynolds number.

To further investigate the asymptotic behavior of $\sqrt{p'^2}$ when normalized by q_0 or τ_w, the spectra are normalized such that the area under the curve represents $\overline{p'^2}/q_0^2$ or $\overline{p'^2}/\tau_w^2$ and are shown in Figs. 8a and 8b, respectively. It can be seen from Fig. 8a that there are two competing effects that contribute to changes in $\sqrt{p'^2}/q_0$ with Reynolds number: a low-frequency effect where the spectrum level decreases with increasing Reynolds number and a high-frequency effect where the spectrum level increases with increasing Reynolds number. The combination of these gives the appearance that the quantity $\sqrt{p'^2}/q_0$ becomes invariant with increasing Reynolds number. However, it is clear that $\sqrt{p'^2}$ does not scale with the dynamic pressure because the spectra in Fig. 8a do not collapse to a single curve.

Figure 8b shows the spectra scaled such that the area under the curve gives the quantity $\overline{p'^2}/\tau_w^2$. It is clear from Fig. 8b that $\sqrt{p'^2}/\tau_w$ increases, albeit slowly, with increasing Reynolds number due to the rise in the energy of the low-frequency region of the spectra. Hence, the quantity $\sqrt{p'^2}/\tau_w$ does not scale, i.e., become Reynolds number independent, on τ_w either but continues to increase slowly with Reynolds number, as was first seen in Fig. 5b. This finding is in agreement with the conclusion of Farabee and Casarella,[1] who utilized their own results along with those from other investigators to show that the ratio $\overline{p'^2}/\tau_w$ increases proportionally to the natural log of Reynolds number based on friction velocity and boundary-layer thickness Re_τ for Re_τ values larger than 333. This logarithmic behavior was predicted earlier by Bradshaw[10] and recently supported in a review paper by Bull.[5]

Figure 6a shows the skewness measured in the current study as a function of Reynolds number. Also plotted are the results of Schewe,[6] Kim,[24] and Karangelen.[23] (Note that Ref. 24 is a DNS of fully developed channel flow at $Re_\tau = 179$.) From Fig. 6a it can be seen that the results of both Schewe[6] and Karangelen[23] indicate that the turbulent wall-pressure fluctuations have a negative skewness of approximately -0.2. In addition, Karangelen indicates that with increasing Reynolds number the skewness begins to approach that of a Gaussian random variable, i.e., zero. However, the current data set shows both negative and positive skewness ranging from approximately -0.05 at the lowest Reynolds number to approximately 0.05 skewness at the highest Reynolds number.

The PDFs for both $Re_\theta = 1577$ and 6241, whose skewness values are equal to -0.05 and 0.05, respectively, are shown, along with a Gaussian PDF, in Fig. 6b. As shown by Fig. 6b, the expected asymmetry in PDFs with a skewness of -0.05 or 0.05 is not evident. Therefore, the conclusion to be drawn is that the skewness values observed in current and previous results of the wall-pressure fluctuations for this Reynolds number based on momentum thickness Re_θ range are essentially equal to zero.

Figure 7 shows the values of kurtosis obtained in the current study as a function of Reynolds number along with the results of Schewe,[6] Kim,[24] and Karangelen.[23] From Fig. 7, it can be seen that there is a general agreement with previously published data. Both the current study and that of Schewe[6] and Karangelen[23] predict a higher flatness value than that of a Gaussian random variable. The current study indicates that the kurtosis of the turbulent wall-pressure signal is consistently around a value of 4.5 for all Reynolds numbers. The data of Karangelen show that the value of kurtosis decreases with increasing Reynolds number, but as stated earlier, the effect of spatial averaging and Reynolds number have not been separated in these results. Hence, it cannot be concluded whether the trend observed in the data of Karangelen is a true Reynolds number effect or a manifestation of the signal attenuation due to spatial averaging.

C. Characteristics of the Wall-Pressure Spectra

Conventionally, investigations of the turbulent boundary-layer scaling issues have predominately focused on inner- and outer-scaling characteristics. It is assumed that the wall layer scales on ν and u_τ, whereas the outer layer of the boundary layer scales with δ (or θ) and u_τ. These are not universally accepted as the proper scales for the turbulent boundary layer, e.g., see Refs. 9, 25, and 26; however, we have used the classical description here. Of course, the inner-layer structures and the outer-layer structures, as well as structures in the overlap region, can contribute to the various frequency ranges of the wall-pressure spectrum. For this investigation,

wall-pressure quantities scaled on inner variables use τ_w, ν, and u_τ to form all of the appropriate length scales and timescales, whereas outer scaling uses τ_w, δ, and u_τ.

1. Comparison of the Wall-Pressure Spectra

Figure 2a shows the wall-pressure spectra obtained in the current investigation at $Re_\theta = 2953$ and 7076 scaled on inner variables. Also plotted are the spectra of Farabee and Casarella,[1] Olivero-Bally et al.,[27] and Schewe.[6] The current results seem to agree very well with those from the other investigations. This is particularly encouraging given that all four investigations were conducted in different facilities and utilizing different measurement techniques. Of particular interest is the agreement with the results from Schewe[6] because he did not use a pinhole in conducting his investigation. This reinforces the argument pointed out by Farabee and Casarella[1] that carefully designed and calibrated pinhole microphones provide accurate measurements of p'. This argument was questioned earlier by Bull and Thomas[16] and more recently by Löfdhal et al.[9]

Löfdhal et al.[9] were able to utilize a flush-mounted MEMS sensor to conduct wall-pressure measurements. The inner-scaled spectrum results from Löfdhal et al. coincided with the measurements of both Farabee and Casarella[1] and Schewe[6] at a single point only. Löfdhal et al.[9] attributed the discrepancy with Farabee and Casarella's results to the utilization of a pinhole in their measurements.[1] However, the same argument could not be used to explain the discrepancy with the results of Schewe[6] (which agree well with Farabee and Casarella's results), who also used a flush-mounted sensor for his investigation. In fact, in a discussion of the Löfdhal et al. paper[9] by Bandyopadhyay et al.,[28] concerns regarding the equilibrium nature of the flowfield of Löfdhal et al. were raised.

The voltage spectra obtained at the lowest and highest Reynolds numbers in this investigation, prior to application of the noise cancellation scheme and microphone calibration, are shown in Fig. 2b. Also plotted is a wind-off spectrum representing the background electrical noise, which sets the limit on the level of pressure fluctuation that can be resolved. It can be seen that the spectrum at $Re_\theta = 7076$ is more than three orders of magnitude above the electronic/ambient noise spectrum for the full frequency range of acquisition. However, the spectrum obtained at the lowest Reynolds number suffers from a poor signal-to-noise ratio at the highest frequencies; therefore, the valid information is contained only at frequencies approximately less than 700 Hz. This is also true for the measurements at $Re_\theta = 1805$ and 1955.

2. Turbulent Source Identification of the Wall-Pressure Spectra

The current investigation examines the scaling characteristics of the turbulent wall-pressure spectrum. Both inner (τ_w, u_τ, ν) and outer (τ_w, u_τ, δ) scaling is implemented to determine which turbulent structures are the dominant motions for a given frequency range in the spectrum.

Figures 9 and 10 show the turbulent wall-pressure spectra obtained using the 0.318-mm pinhole normalized on inner and outer variables, respectively. Figure 9a contains all of the spectra of the current investigation scaled on inner variables. Figure 10 shows the same spectra but normalized using outer variables. In Fig. 9a, for the frequency range of $\omega^+ < 0.1$, the inner-scaled spectra show a Reynolds number variation where the energy content of the spectra increases with increasing Reynolds number. This effect can be better seen in Fig. 9b, where only three cases are plotted. Note that the horizontal error bar in Fig. 9b represents an uncertainty of ±6% along the ω^+ axis due to normalization by u_τ, whose uncertainty is ±3%, as discussed in Sec. II.C. A similar error bar along the $\phi^+_{p'p'}$ axis is unnoticeable because of the linear scale.

In Fig. 10, the corresponding frequency range, when normalized on outer variables, is approximately $\omega^o < 70.0$. In this frequency range the spectra collapse to a single curve. This indicates that the low-frequency range of the turbulent spectra scales on outer variables and that the pressure fluctuations associated with the large-scale motion dominate that region of the spectrum. A second feature is the peak in the turbulent spectra when scaled on outer variables. Although the peak region is rather broad, it is observed at a nondimensional frequency of $\omega^o \approx 55.0$ for all Reynolds numbers. This result is in agreement with the observations made by Farabee and Casarella,[1] who found the peak in the turbulent spectra to occur at $\omega^o = 50$.

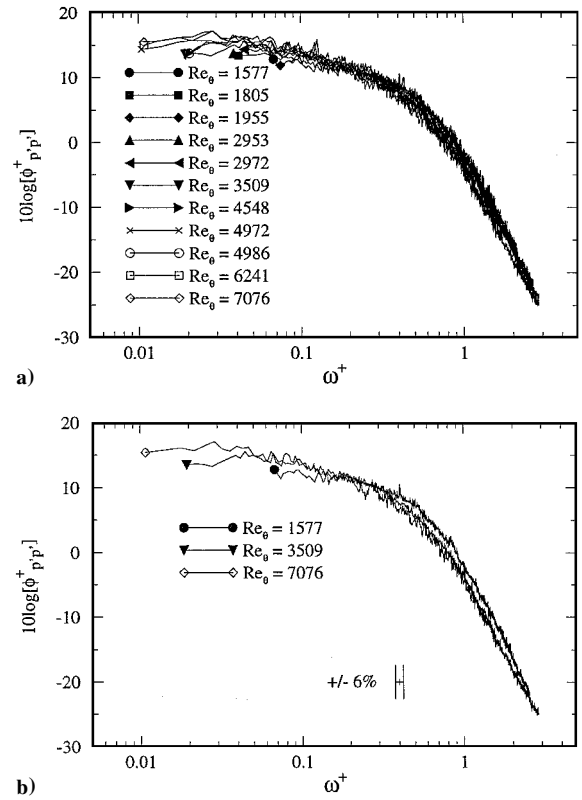

Fig. 9 Wall-pressure spectra obtained under the 0.318-mm-diam pinhole scaled on inner variables: a) all of the cases and b) three cases to demonstrate the Reynolds number variation in the low-frequency region.

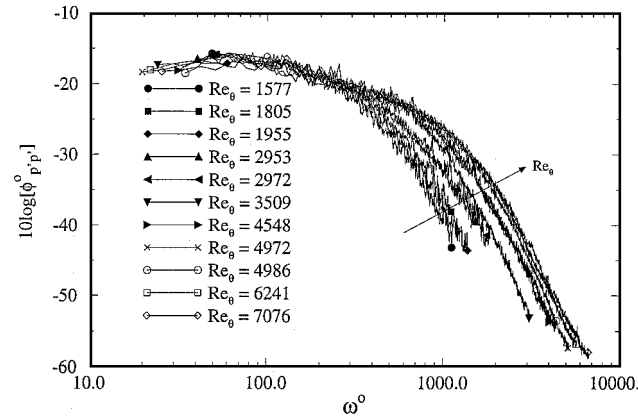

Fig. 10 Wall-pressure spectra obtained under the 0.318-mm-diam pinhole scaled on outer variables.

The spectra, for the range of Reynolds numbers investigated, collapse to a single curve when scaled on inner variables for $\omega^+ > 0.2$ or when scaled on outer variables for $\omega^o < 200.0$ (Figs. 9 and 10). This region is typically referred to as the overlap region. It can be shown that the size of a turbulent eddy that scales with both inner and outer variables is proportional to the location of the eddy above the wall. In other words, the length scale of such a turbulent eddy scales on its height y in the boundary layer. These eddies are known as attached eddies[29] and have been argued, e.g., by Perry et al.,[30] to be the dominant turbulent motion in the logarithmic part of the boundary layer. Thus, it is reasonable to expect the contribution to the spectra in the middle-frequency range to be primarily due to turbulent motions in the logarithmic part of the boundary layer. This conclusion has also been pointed out by Farabee and Casarella.[1] As discussed by Panton,[12] the lower bound, in ω^+, and the upper bound, in ω^o, for the overlap region is Reynolds number dependent.

In other words, for increasing Reynolds number a larger range of the spectra collapses on both inner and outer variables.

The third frequency range of interest begins at the end of the overlap region and shows that the wall-pressure spectra collapse when scaled on inner variables but exhibit a Reynolds number trend when normalized by outer variables, where the energy level increases with increasing Reynolds number. This trend is also in agreement with that observed by Farabee and Casarella.[1]

3. Power Law Features in the Wall-Pressure Spectra

In addition to the scaling characteristics, the shape of the turbulent spectrum is used by researchers to develop models of the wall-pressure signature. Over the years, different researchers have shown, using scaling arguments, that the wall-pressure spectrum for a certain frequency range should obey a power-law type of behavior, i.e., $\phi_{p'p'}(\omega) \sim \omega^n$, where n is dependent on the frequency range of the turbulent spectrum.

The scaling analyses by Bradshaw[10] and Panton and Linebarger[11] predict a region where the spectra collapse on both inner and outer variables. In addition, they have shown that this region should exhibit an ω^{-1} behavior and it can be associated with pressure sources in the logarithmic part of the boundary layer. Figure 11 shows spectra obtained at $Re_\theta = 1577$ (left-hand panel) and $Re_\theta = 7076$ (right-hand panel) scaled on inner variables. From Fig. 11 (right-hand panel), it can be seen that the current results show that a rather significant portion of the spectrum exhibits an ω^{-1} behavior for $0.16 < \omega^+ < 0.4$. Recall that the lower bound, in ω^+, is Reynolds number dependent. Therefore, the frequency range over which the spectra exhibits the ω^{-1} behavior decreases with decreasing Reynolds number. This is seen in Fig. 11 (left-hand panel), where the extent of the ω^{-1} region is smaller or even nonexistent. Recent results from Olivero-Bally et al.[27] also show a significant region of ω^{-1} over the frequency range of $0.07 < \omega^+ < 0.5$ that is in agreement with the current study. In addition, the current results are in agreement with the results of Farabee and Casarella[1] in that both investigations show an overlap region. However, Farabee and Casarella do not show as wide of a range of ω^{-1} behavior, possibly due to the noise cancellation scheme used in their investigation.[15]

Monin and Yaglom[13] theorized an $\omega^{-7/3}$ behavior for locally isotropic turbulence. More recently, Olivero-Bally et al.[27] have shown that this portion of the spectrum receives contributions from pressure sources in the highest part of the buffer zone of the boundary layer. In Fig. 11, it can be seen that there is a small region in the turbulent wall-pressure spectra that exhibits this behavior for the frequency range of $0.4 < \omega^+ < 0.7$. This is in agreement with Schewe,[6] who observed this power law behavior over the range $0.4 < \omega^+ < 0.8$, and with Olivero-Bally et al.,[27] who also show this behavior for the frequency range of $0.5 < \omega^+ < 1.0$. However, one could debate whether a $-\frac{7}{3}$ slope exists in the present data. We show a $-\frac{7}{3}$ slope on the spectrum plot for the sake of completeness and comparison with the results of other researchers.

Finally, Blake[14] theorized an ω^{-5} scaling behavior in the high-frequency region of the turbulent wall-pressure spectrum. He associated this behavior with sources in the boundary layer below $y^+ = yu_\tau/\nu \sim 20$ (Ref. 27). The current results show this ω^{-5} behavior for the frequency range of $1.0 < \omega^+ < 3.0$ (Fig. 11) and are in agreement with the ω^{-5} region observed by Olivero-Bally et al., whose spectra exhibited this behavior for the frequency range of $1.0 < \omega^+ < 1.6$.

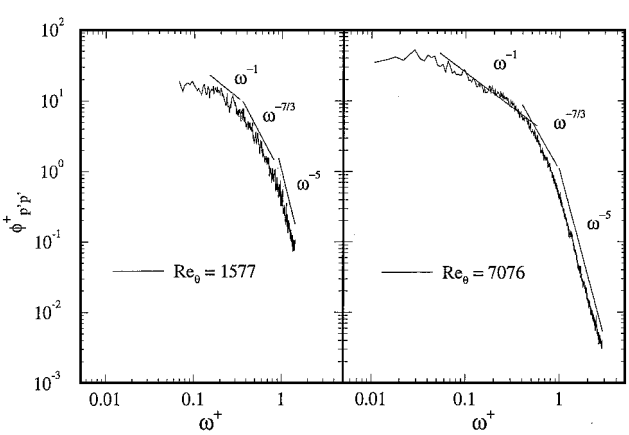

Fig. 11 Power law features present in the wall-pressure spectra.

IV. Conclusions

The effect of spatial averaging on wall-pressure measurements was studied by measuring the wall-pressure fluctuations with a microphone under pinholes of various size in the range $2 \le d^+ \le 27$. It was found that the maximum allowable nondimensional sensing diameter to avoid spectral attenuation for frequencies up to $f^+ = f\nu/u_\tau^2 = 1$ is in the range $12.0 \le d^+ < 18.0$. This spectral attenuation resulted in a barely observable reduction in the overall rms level of the wall pressure for $d^+ < 27.0$. For the same sensor size range, it was also shown that there was no significant effect on the skewness and kurtosis.

The variation of turbulent wall-pressure statistics with Reynolds number was also studied. It was found that both $\sqrt{\overline{p'^2}}/q_0$ and $\sqrt{\overline{p'^2}}/\tau_w$ varied with Reynolds number and that scaling of the spectra has shown that the structures responsible for the generation of the pressure fluctuations at the wall do not scale with the freestream velocity or the wall shear stress. Also, it was found that the wall-pressure fluctuations have a kurtosis value of approximately 4.5, which is larger than a Gaussian variable, and skewness very close to zero.

Turbulent source identification by spectral scaling methods has indicated that turbulence activity in the outer part of the boundary layer is responsible for the contribution to the low-frequency range of the wall-pressure spectrum. In addition, the middle-frequency range of $\phi_{p'p'}$ is seen to scale on both inner and outer variables, indicating that pressure sources in the logarithmic layer are responsible for contributions to this region of the spectrum. Finally, the high-frequency region of the spectra was seen to scale on inner variables, indicating that the wall region of the boundary layer is the dominant source of the high-frequency pressure fluctuations. These findings agree with previously published results.

Turbulent wall-pressure spectra exhibited the power law behavior predicted by previous researchers. Specifically the spectra were shown to have a -1 slope for the frequency range of $0.16 < \omega^+ < 0.4$. Furthermore, an ω^{-5} behavior was seen in the high-frequency region of the spectra for $1.0 < \omega^+ < 3.0$.

Acknowledgments

The authors would like to thank the Office of Naval Research under Contract ONR N00014-93-1-0639, monitored by Pat Purtell, and NASA Space Grant–Aerospace Illinois for sponsoring the current investigation.

References

[1] Farabee, T. M., and Casarella, M. J., "Spectral Features of Wall Pressure Fluctuations Beneath Turbulent Boundary Layers," *Physics of Fluids A*, Vol. 3, No. 10, 1991, pp. 2410–2420.

[2] Wambsganss, M. W., and Zaleski, P. L., "Measurements, Interpretation and Characterization of Near Field Flow Noise," Argon National Lab., Rept. ANL-7685, 1970, pp. 112–140.

[3] Willmarth, W. W., "Pressure Fluctuations Beneath Turbulent Boundary Layers," *Annual Review of Fluid Mechanics*, Vol. 7, 1975, pp. 13–38.

[4] Eckelmann, H., "A Review of Knowledge on Pressure Fluctuations," *Near-Wall Turbulence*, edited by S. J. Kline and N. H. Afgan, Hemisphere, New York, 1990, pp. 328–347.

[5] Bull, M. K., "Wall-Pressure Fluctuations Beneath Turbulent Boundary Layers: Some Reflections on Forty Years of Research," *Journal of Sound and Vibrations*, Vol. 190, No. 3, 1996, pp. 299–315.

[6] Schewe, G., "On the Structure and Resolution of Wall-Pressure Fluctuations Associated with Turbulent Boundary Layer Flow," *Journal of Fluid Mechanics*, Vol. 134, Sept. 1983, pp. 311–328.

[7] Lueptow, R. M., "Transducer Resolution and the Turbulent Wall Pressure Spectrum," *Journal of the Acoustical Society of America*, Vol. 97, No. 1, 1995, pp. 370–378.

[8] Kim, J., Moin, P., and Moser, R. D., "Turbulence Statistics in Fully Developed Channel Flow and Low Reynolds Number," *Journal of Fluid Mechanics*, Vol. 177, March 1987, pp. 133–166.

[9]Löfdahl, L., Kälvesten, E., and Stemme, G., "Small Silicon Pressure Transducers for Space–Time Correlation Measurements in a Flat Plate Boundary Layer," *Journal of Fluids Engineering*, Vol. 118, No. 3, 1996, pp. 457–463.

[10]Bradshaw, P., "Inactive Motion and Pressure Fluctuations in Turbulent Boundary Layers," *Journal of Fluid Mechanics*, Vol. 30, No. 2, 1967, pp. 241–258.

[11]Panton, R. L., and Linebarger, J. H., "Wall Pressure Spectra Calculations for Equilibrium Boundary Layers," *Journal of Fluid Mechanics*, Vol. 65, No. 2, 1974, pp. 261–287.

[12]Panton, R. L., "Inner-Outer Structure of the Wall-Pressure Correlation Function," *Near-Wall Turbulence*, edited by S. J. Kline and N. H. Afgan, Hemisphere, New York, 1990, pp. 381–396.

[13]Monin, A. S., and Yaglom, A. M., *Statistical Fluid Mechanics*, Vol. 2, MIT Press, Cambridge, MA, 1975, pp. 375–377.

[14]Blake, W. K., *Mechanics of Flow-Induced Sound and Vibration*, Academic, New York, 1986, pp. 497–588.

[15]Naguib, A. M., Gravante, S. P., and Wark, C. E., "Extraction of Turbulent Wall-Pressure Time-Series Using an Optimal Filtering Scheme," *Experiments in Fluids*, Vol. 22, No. 1, 1996, pp. 14–22.

[16]Bull, M. K., and Thomas, A. S. W., "High Frequency Wall-Pressure Fluctuations in Turbulent Boundary Layers," *Physics of Fluids*, Vol. 19, No. 5, 1976, pp. 597–599.

[17]Wark, C. E., and Nagib, H. M., "Experimental Investigation of Coherent Structures in Turbulent Boundary Layers," *Journal of Fluid Mechanics*, Vol. 230, Sept. 1991, pp. 183–208.

[18]Snarski, R. S., "Relation Between the Fluctuating Wall Pressure and the Turbulent Structure of a Boundary Layer on a Cylinder in Axial Flow," Ph.D. Thesis, Dept. of Mechanical Engineering, Northwestern Univ., Evanston, IL, Dec. 1992.

[19]Gravante, S. P., "Reynolds Number Effects on Time-Resolved Measurements of the Wall Pressure Beneath a Turbulent Boundary Layer," M.S. Thesis, Dept. of Mechanical and Aerospace Engineering, Illinois Inst. of Technology, Chicago, IL, July 1995.

[20]Naguib, A. M., "Inner- and Outer-Layer Effects on the Dynamics of a Turbulent Boundary Layer," Ph.D. Thesis, Dept. of Mechanical and Aerospace Engineering, Illinois Inst. of Technology, Chicago, IL, Dec. 1992.

[21]Hites, M. H., "Scaling of High-Reynolds Number Turbulent Boundary Layers in the National Diagnostic Facility," Ph.D. Thesis, Dept. of Mechanical and Aerospace Engineering, Illinois Inst. of Technology, Chicago, IL, May 1997.

[22]Karangelen, C. C., Wilczynsi, V., and Casarella, M. J., "Large Amplitude Wall Pressure Events Beneath a Turbulent Boundary Layer," *Journal of Fluids Engineering*, Vol. 115, No. 3, 1993, pp. 653–659.

[23]Karangelen, C. C., "Temporal and Spectral Features of Wall-Pressure Fluctuations Beneath a Turbulent Boundary Layer," Ph.D. Thesis, Catholic Univ. of America, Washington, DC, 1991.

[24]Kim, J., "On the Structure of Pressure Fluctuations in Simulated Turbulent Channel Flow," *Journal of Fluid Mechanics*, Vol. 205, Aug. 1989, pp. 421–451.

[25]George, W. K., Knecht, P., and Castillo, L., "The Zero Pressure Gradient Boundary Layer Revisited," 13th Symposium on Turbulence, Rolla, MO, Sept. 1992.

[26]Keith, W. L., Hurdis, D. A., and Abraham, B. M., "A Comparison of Turbulent Boundary Layer Wall-Pressure Spectra," *Journal of Fluids Engineering*, Vol. 114, No. 2, 1992, pp. 338–347.

[27]Olivero-Bally, P., Forestier, B. E., Focquenoy, E., and Olivero, P., "Wall-Pressure Fluctuations in Natural and Manipulated Turbulent Boundary Layers in Air and Water," American Society of Mechanical Engineers Winter Meeting, New Orleans, LA, Nov. 1993.

[28]Bandyopadhyay, P. R., Panton, R. L., Farabee, T. M., Keith, W. L., and Casarella, M. J., "Discussion: Small Silicon Pressure Transducers for Space–Time Correlation Measurements in a Flat Plate Boundary Layer," *Journal of Fluids Engineering*, Vol. 118, No. 4, 1996, pp. 879–881.

[29]Townsend, A. A., *The Structure of Turbulent Shear Flow*, Cambridge Univ. Press, London, 1976, pp. 106–120.

[30]Perry, A. E., Henbest, S., and Chong, M. S., "A Theoretical and Experimental Study of Wall Turbulence," *Journal of Fluid Mechanics*, Vol. 67, No. 2, 1986, pp. 257–271.

F. W. Chambers
Associate Editor